June 4, 1986

Semiannual Status Reports
Covering the Period from December 1, 1985 to May 31, 1986
Grant No. NAGW-661

Measurements of HO_2 Chemical Kinetics with a New Detection Method

BY:

Long C. Lee and Masako Suto
Department of Electrical & Computer Engineering
San Diego State University
San Diego, CA 92182

Prepared for:

NASA Headquarters
Washington, D. C. 20546
Attention: Dr. R. F. Hampson
Code EE

I. Introduction

This report covers the period from December 1, 1985 to May 31, 1986 for the research program currently supported by NASA under Grant No. NAGW-661 basic. In this program, the reaction rate constant of HO_2+O_3 has been measured with a discharge-flow-tube apparatus. The HO_2 radical was detected by the OH(A-X) photofragment emission produced from photodissociative excitation of HO_2 at 147 nm. In the meantime, the optical emissions produced by the vacuum ultraviolet excitation of chemical species in the flow tube were investigated and used to examine the possibility for their interference with the HO_2 detection. The research results are summarized below.

II. Research Accomplished

A. Reaction Rate Constant of HO_2+O_3

A discharge-flow-tube apparatus has been constructed and used to measure the reaction rate constant of HO_2+O_3. The flow tube consisted of three coaxial tubes. The innermost tube was a movable Teflon tube of 2 mm ID, and the second tube was a movable Teflon coated Pyres tube of 1 cm ID and 70 cm long. The main reactor was a Teflon coated Pyres tube. Two sizes of tubes were used - one 4.8 cm ID and the other 2.2 cm ID.

HO_2 was produced by the reaction sequence:

$$Cl + CH_3OH \rightarrow CH_2OH + HCl$$

$$CH_2OH + O_2 \rightarrow HO_2 + CH_2O$$

The Cl atom was produced by microwave discharge of a trace amount of Cl_2 in He. The HO_2 was detected by monitoring the

OH(A-X) emission from photodissociative excitation of HO_2 by a Xe resonance light at 147 nm,

$$HO_2 + h\nu(147\ nm) \rightarrow OH(A^2\Sigma^+) + O$$

$$OH(A^2\Sigma^+) \rightarrow OH(X^2\Pi) + h\nu\ (306\text{-}320\ nm).$$

The concentrations of Cl and the consequent reaction products (such as CH_2OH, CH_2O and HO_2) were limited to low values such that the requirements for the pseudo-first-order reaction were satisfied. HO_2 could be regenerated by the reaction sequence:

$$HO_2 + O_3 \rightarrow OH + 2O_2$$

$$OH + O_3 \rightarrow HO_2 + O_2$$

The regeneration was greatly reduced by adding C_2F_3Cl or C_3H_8 as the OH scavenger.

The reaction rate of $HO_2 + O_3$ at room temperature was measured as a function of reaction time and O_3 concentration. The reaction rate constants measured with different flow tubes sizes and different OH scavengers are consistent to be $(1.9 \pm 0.3) \times 10^{-15}$ cm^3/s. A computer simulation modeling for the reaction kinetics occurring in the flow tube was carried out to confirm that the secondary reactions were negligible at the low HO_2 concentrations used in the experiment. This current reaction rate constant agrees very well with the value of 2×10^{-15} cm^3/s measured by the Laser-magnetic-resonance technique. Our results are described in more detail in a paper entitled "Reaction Rate Constant of HO_2+O_3 Measured by Detecting HO_2 from Photofragment Fluorescence" which is attached in this report as Appendix A.

We are measuring the HO_2+O_3 reaction rate constant in the temperature range of 200-350 ^oC. The result will be presented in the next report.

B. Photofragment Emissions for VUV Excitation of Chemical Species in the Flow Tube

When the chemical species in the flow tube are excited by the 147 nm photons, they may produce UV light to interfere with the OH(A-X) emission from photoexcitation of HO_2. Thus, the optical emissions from the vacuum ultraviolet (VUV) excitation of chemical species in the flow tube are needed to interpret our data. The fluorescence spectra of various chemical species were investigated using synchrotron radiation as a light source. The emission spectra were also produced by excitation of the chemical species with intense atomic lines, and they were dispersed to identify the emitting species.

The OH(A-X) emission from photoexcitation of CH_3OH has been observed and the result has been reported in an earlier paper (J. B. Nee, M. Suto and L. C. Lee, Chem. Phys. 98, 147 (1985)). The result for photoexcitation of Cl_2 has been recently published in the Journal of Chemical Physics which is attached in this report as Appendix B. The spectroscopic data of HCl, CH_2O, C_3H_8 and C_2F_3Cl have been obtained and analyzed. Their results will be summarized in papers and published in scientific journals. Among all these molecules studied, only C_2F_3Cl emits at 147 nm. The cross section for the emission in the 300-330 nm region is, however, quite small such that this emission does not seriously

disturb the measurement of HO_2 concentration by the photofragment emission method.

In summary, the photofragment emissions of all chemical species in the flow tube have been investigated, and their possible interferences to the OH(A-X) emission produced by photoexcitation of HO_2 have been examined. It is concluded that the possible optical emissions from other chemical species do not interfere the measurement of HO_2 concentration by the photofragment emission method. Thus, our measurement of the HO_2+O_3 reaction rate constant is not affected by the optical emissions from chemical species other than HO_2.

Appendix A

"Reaction Rate Constant of HO_2+O_3 Measured by Detecting HO_2 from Photofragment Fluorescence"

Reaction Rate Constant of HO_2+O_3 Measured by Detecting HO_2 from Photofragment Fluorescence

E. R. Manzanares, Masako Suto, and Long C. Lee
Department of Electrical & Computer Engineering
San Diego State University
San Diego, CA 92182

and

DeWitt Coffey, Jr.
Department of Chemistry
San Diego State University
San Diego, CA 92182

ABSTRACT

The rate constant for the reaction $HO_2+O_3 \rightarrow OH+2O_2$ was investigated in a discharge-flow system at room temperature. HO_2 was produced from the reaction sequence: $Cl+CH_3OH \rightarrow CH_2OH+HCl$ and $CH_2OH+O_2 \rightarrow HO_2+CH_2O$. HO_2 was detected by the OH(A-X) fluorescence produced from photodissociative excitation of HO_2 at 147 nm. A computer modeling of the reaction kinetics occurring in the flow tube was carried out to confirm that contributions from secondary reactions were negligible at low HO_2 concentrations. The rate constant was determined from first order decay of HO_2 in excess O_3. The measured reaction rate constant of HO_2+O_3 is $(1.9 \pm 0.3)\times10^{-15}$ cm^3/s, which agrees well with published data.

I. INTRODUCTION

The reaction of odd hydrogen radicals, in particular, the reaction sequence

$$HO_2 + O_3 \rightarrow OH + 2O_2 \quad (1)$$

$$OH + O_3 \rightarrow HO_2 + O_2 \quad (2)$$

has been implicated as major depletion reactions for O_3 in the lower stratosphere and important radical reactions in the troposphere. Several direct measurements of k_2 have been undertaken[1-3] but to date only the laser magnetic resonance (LMR) detection[4] of HO_2 has been employed to directly measure k_1. In this present study, we demonstrate that the discharge-flow technique with photofragment emission (DF-PE) detection[5,6] of HO_2 can be used to directly measure the rate constant of reaction (1).

HO_2 was produced by microwave discharge of Cl_2, which then reacted with CH_3OH and O_2 by[6]

$$Cl + CH_3OH \rightarrow CH_2OH + HCl \quad (3)$$

$$CH_2OH + O_2 \rightarrow HO_2 + CH_2O \quad (4)$$

HO_2 was detected by monitoring the $OH(A^2\Sigma^+ \rightarrow X^2\Pi)$ emission from photodissociative excitation of HO_2 by a Xe resonance light at 147 nm,[6]

$$HO_2 + h\nu \ (147 \text{ nm}) \rightarrow OH(A^2\Sigma^+) + O \quad (5)$$

$$OH(A^2\Sigma^+) \rightarrow OH(X^2\Pi) + h\nu \ (306\text{-}320 \text{ nm}) \quad (6)$$

The experimental conditions were such that the requirements for psuedo-first order reaction were satisfied. Regeneration of HO_2 via reaction (2) was greatly reduced by adding OH scavengers.[4,7] Two reagents, C_2F_3Cl and C_3H_8, were used as OH

scavengers in our experiments.

Since the measurement of reaction rate constant involves many experimental parameters, it is essential to apply different techniques to verify agreement among reported values. Both the methods of production and detection of HO_2 for the study of reaction (1) in this experiment are different from previously reported experiments.[4,7-9] This work reports the second direct measurement for the rate constant of reaction (1).

II. EXPERIMENTAL

The schematic diagram of the experimental apparatus is shown in Fig. 1. The experimental chamber consisted of a flow tube assembly and a gas cell. The flow tube consisted of three coaxial tubes. The innermost tube was a movable teflon tube of 2 mm i.d. through which CH_3OH and O_2 were fed. The second tube, a teflon coated Pyrex, was also a movable injector of 1 cm i.d. and 70 cm long. Chlorine atoms were produced upstream by a microwave discharge of a trace of Cl_2 in He. Helium was also used as a carrier gas and its flow rate (Q_1) was regulated by a mass flow controller (MKS instruments). The production of HO_2 was completed in this tube.

The main reactor was also a teflon coated Pyrex tube. Two sizes were used, one of 4.8 cm i.d. and the other 2.2 cm i.d. both 60 cm long. O_3 and the OH scavenger, C_2F_3Cl or C_3H_8, were introduced into the flow tube upstream. O_3 was produced, prior to use, by a high voltage a.c. discharge of O_2 at atmospheric pressure and stored on two silica gel traps at 195 ^oK. The O_3 was purified before use by pumping on the silica gel O_3 traps

down to a few torr, where the O_3 concentration measured by absorption of 253.7 nm agreed with the pressure measured by an MKS Baratron manometer. O_3 was introduced into the flow tube with He as a carrier gas with the He flow rate (Q_2) regulated by another controller. The elution rate of O_3 was controlled by varying both the flow rate and the temperature of the trap. The partial pressure of O_3 was monitored by the attenuation of the 253.7 nm Hg line at two positions, upstream of the flow tube and downstream after the gas cell. Both measurements agreed within experimental uncertainty, indicating O_3 loss in the flow tube was negligible.

HO_2 radicals reacted with O_3 in the main reaction tube. The partial pressure of all gases were fixed, and the reaction times were varied by moving the position of the HO_2 injector tube. The reaction time is a function of the linear flow velocity which in turn is dependent on the total flow rate. The total flow rate (discussed in detail below) was determined for the flow conditions of each experimental run. The pressures in the flow tube and in the gas cell were monitored separately by two Baratron manometers (MKS). The ratio of total pressures $(P_{tube}-P_{cell})/P_{cell} \sim 0.05$. Since the pressure drop was so small, no corrections for Poiseuille drop were made (discussed in Section C of Results).

The carrier gas was in excess over the reactants, so the total flow rate was dependent largely on the He flow rate. The total flow rate was determined as follows. First, the volume of the chamber, V_T, was determined using Boyle's Law with a calibrated (at room temperature) 1000 cm^3 container as a

reference volume, V_1. A known pressure of He, P_1, was contained in V_1 and then expanded to the total volume, $V_2 = V_T + V_1$, and the pressure in V_2, P_2, was recorded. Thus, $V_2=P_1V_1/P_2$ in cm^3. With the flow rates of He, Q_1 and Q_2, kept constant, the chamber was isolated from the pump and the increase in pressure per min, $\Delta P/\Delta t$ in torr/min, was recorded. The total standard flow rate, Q_T, was obtained using:

$$Q_T = V_2 (273/760) (\Delta P/\Delta t)/T \qquad (8)$$

where T is temperature in K, and Q_T is the flow rate in standard cubic centimeter per minute (SCCM). This equation was used to verify the instrumental flow rate settings Q_1 and Q_2. For the kinetic experiments, the ratio of $\Delta P/\Delta t$ was determined for each individual run with all the major reactants in the flow as well.

The linear flow velocity in the tubes was derived from:

$$v = V_2 [(\Delta P/\Delta t)/(60P)] (1/\pi r^2) \qquad (9)$$

where P is the total pressure, $P = (P_{tube}+P_{cell})/2$, at which the experiment was performed, r is the radius of the flow tube and v is in cm/sec. The error estimates at 95% confidence level[10] are: V_2 (± 2%), T (± 1%), P (± 5%), $\Delta P/\Delta t$ (± 7%), and r (± 1%). The resultant error in Q_T or v is ± 9%. The total flow rates were typically in the range of 150-250 SCCM with the 4.8 cm i.d. and 80-100 SCCM with the 2.2 cm i.d., for which the linear flow velocities in the main reaction flow tube were in the range 100-130 cm/s and 150-200 cm/s, respectively.

The gas cell was a six-way-stainless steel-cross of 3 inch o.d. HO_2 radicals were detected by monitoring its $OH(A \rightarrow X)$ photofragment emission. A sealed Xe resonance lamp with a MgF_2 window was used as a light source. The light source intensity

was monitored by a CsI photodiode (Hamamatsu R1187). A gas filter (1% CH_4 in Ar at atmospheric pressure) was used to cut-off the 129.5 nm line in the Xe lamp so that only the 147 nm line transmitted into the gas cell.[6] The OH(A-X) emission from HO_2 was detected at the direction perpendicular to both the light source and the gas flow by a cooled PMT (EMI 9558 QB). A narrow band pass filter (310 ± 10 nm) was used to isolate the OH(A-X) band. The signal from the PMT was processed by an ORTEC counting system and the output fed to an IBM PC. The carrier gas flow rates, the total pressure, and the intensities of the 147 nm and 253.7 nm light sources were also simultaneously recorded by the computer.

The gas mixture of 2.0% Cl_2 in He and the lecture bottles of C.P. grade C_2F_3Cl (> 99.0%) and C_3H_8 (> 99.0%) were supplied by Matheson. The CH_3OH (supplied by Fisher, purity > 99.9%) vapor was carried by He into the gas cell. The concentration of CH_3OH was determined from the ratio of the CH_3OH vapor pressure (120 torr at room temperature) to the pressure of the carrier gas. O_2 was supplied by Amerigas and He of UHP grade (99.999%) was supplied by M.G. Scientific. Gases were used as delivered.

III. RESULTS AND DISCUSSION

A. Detection of HO_2 Radicals

The photofragment emission intensity can be described by,

$$I_f = C\sigma_f[HO_2]\, I_o \exp(-\sigma_i n_i \ell)/(1 + \tau \textstyle\sum_i n_i k_i), \qquad (7)$$

where C is a constant including the geometric factor and the PMT detection efficiency, σ_f is the cross section for the OH(A → X)

fluorescence produced from excitation of HO_2 at 147 nm, $[HO_2]$ is the HO_2 concentration, I_o is the light source intensity of the Xe lamp, ℓ is the path length of the light source from the MgF_2 window to the center of the PMT view region, τ is the radiative lifetime of the OH(A-X) transition; n_i, σ_i and k_i are the concentrations, the absorption cross sections at 147 nm, and the quenching rate constants of OH*(A) by various species in the flow tube, respectively. The exponential term represents the attenuation of the light source intensity at 147 nm by various species in the flow tube. The denominator represents the reduction in OH emission by the quenching of OH*(A) by the various gases.

The absorption cross sections for O_2, O_3, CH_3OH, C_2F_3Cl, and C_3H_8 at 147 nm were determined from the slope of the linear plot of absorbance versus pressure for each gas and are 1.4×10^{-17}, 4.41×10^{-18}, 1.30×10^{-17}, 1.80×10^{-17} and 7.67×10^{-18} cm^2, respectively. The absorption cross-section[11] of Cl_2 is $< 10^{-18}$ cm^2. The attenuation of light source intensity by all gases for the optical path from the MgF_2 window to the detection region of about 1 cm was estimated to be about 10% at a typical experimental condition such as $[O_3] = 2.5 \times 10^{15}$ cm^{-3}, $[O_2] = 1.0 \times 10^{15}$ cm^{-3}, $[CH_3OH] = 1.0 \times 10^{14}$ cm^{-3}, $[Cl_2] = 6.5 \times 10^{13}$ cm^{-3} and $[C_2F_3Cl] = 4 \times 10^{15}$ cm^{-3} (or $[C_3H_8] = 6.5 \times 10^{15}$ cm^{-3}).

The quenching term ($\tau \sum_i n_i k_i$) of OH*(A) by all gases in the flow tube is estimated to be about 1.6 and 2.6 with C_2F_3Cl and C_3H_8 as scavengers, respectively, assuming that the quenching rate constants of OH*(A) by all the gases are equal to the gas kinetic constant (3×10^{-10} cm^3/s). The OH(A-X) emission intensity

may thus be reduced by a factor of 2.6 or 3.6, depending on C_2F_3Cl or C_3H_8 being used as the OH scavenger. With such attenuation, the light source intensity was still strong enough for the detection of HO_2 radicals.

The photofragment emissions in the UV region from photoexcitation of various gases used in this experiment were also studied. The OH(A-X) emission was observed from excitation of CH_3OH at 147 nm with fluorescence cross section[12] of 3×10^{-21} cm^2. An intense photofragment emission in the UV region (280-380 nm) was observed from excitation of C_2F_3Cl at 147 nm. The fluorescence cross section of C_2F_3Cl has been measured in the 105-170 nm region;[13] however, when a narrow bandpass filter (310 ± 10 nm) was used, the fluorescence signal was greatly reduced such that it only contributed a small constant background. The other molecules do not fluoresce in the UV region when excited at 147 nm.

From the above results, it is conclusive that the relative HO_2 concentration in the gas cell can be measured from the OH(A-X) emission. The estimated minimum detectable $[HO_2]$ is $\sim 10^9$ molecule/cm^3. In each measurement of the $HO_2 + O_3$ reaction rate, flow conditions, which included gas flow velocities, gas flow rates, gas pressures, and microwave discharge power were fixed, except for the reaction time which was varied by changing the position of the movable injector. Since the gas pressures in each measurement were kept constant, the light attenuation, quenching, and emission due to species other than HO_2 were constant so that the relative $[HO_2]$ is proportional to the OH(A-

X) fluorescence intensity observed. For a fixed [O_3], relative [HO_2] was measured as a function of the reaction time.

B. HO_2 Concentrations and Secondary Reactions

The calibration of HO_2 by reaction with NO to give NO_2 and OH, where the [OH] was measured by OH(A-X) resonance fluorescence,[5] proved difficult for this chemical system. Instead, the [HO_2] was estimated by a titration method using CH_3OH as titrant and the data were compared with a kinetic model. For [Cl_2] = 5.5×10^{13} cm^{-3} and [O_2] = 1.3×10^{15} cm^{-3} kept constant, the data of I_f versus [CH_3OH] are plotted in Fig. 2 for two reaction times, 45 and 65 msec, inside the central tube (1 cm i.d.) and for an additional 10 and 20 msec to the detection region, respectively. The error bars in I_f represent one standard deviation and that in [CH_3OH] is the instrumental uncertainty of the pressure manometer. The reactions for the kinetic model are summarized in Table 1. The calculations were carried out using a program which uses the Gear routine for the solution of differential equations.[14]

The reactions in the model are similar to those considered by Takacs and Howard in their modeling of the self-reaction of HO_2.[15] The estimates for the wall losses were deduced from other experimental data. Wall loss rate for HO_2 was not greater than 1.5 s^{-1} in the central tubing (deduced from the intercepts of Figs. 9-11 as discussed later). When the O_2/CH_3OH injector was positioned so that the residence time of Cl was about 40 msec before interacting with CH_3OH and O_2, no fluorescence from HO_2 was detected, thus an upper limit to Cl loss rate is 25 s^{-1}. The wall loss rate of CH_2OH was estimated to be 185 s^{-1} for a

halocarbon wax coated tube of 1.24 cm i.d. at comparable flow velocities used in our experiments.[6]

In the modeling, at each [CH_3OH], the [O_2] was given and [Cl] was varied to give the best fit to the data. Best agreement was obtained between computer calculations and experiments when $1x10^{11}$ < [Cl] < $2x10^{11}$ cm^{-3} and wall loss rate of Cl was 10 s^{-1}. Wall loss rates of HO_2 and CH_2OH contributed insignificantly to the curve fitting. Experimental and calculation data were normalized at [CH_3OH] = $1x10^{14}$ cm^{-3} and compared in Fig. 2.

First, ignoring wall losses of HO_2, Cl and CH_2OH, plots (a) and (b) of Fig. 2 are the simulation curves with [Cl] = $1x10^{11}$ and $2x10^{11}$ cm^{-3}, respectively. Plot (c) is with $k_w(HO_2)$ = 1.5 s^{-1} for [Cl] = $1x10^{11}$ cm^{-3}. There is no substantial change in the simulation curve when $k_w(HO_2)$ is considered. The same curve as (c) was obtained when $k_w(CH_2OH)$ = 200 s^{-1} was included in the modeling. Curve (d) is obtained when $k_w(Cl)$ = 10 s^{-1} and $k_w(CH_2OH)$ and $k_w(HO_2)$ were set at zero. Including $k_w(Cl)$ improved the curve fitting at smaller [CH_3OH]. However, the change in curve (d) was not significant when wall losses from HO_2 and CH_2OH were considered. The [Cl] represents the Cl entering the central reactor. The amount of Cl formed in the discharge region is possibly high but wall losses and atom recombination can also be high so that the resulting [Cl] is low.

Complications in the treatment of our kinetic data for the HO_2 + O_3 reaction could arise from (i) interference of the OH fluorescence from photodissociation of H_2O_2 and (ii) contributions from secondary reactions. These are discussed

below.

H_2O_2 is produced in the reaction of HO_2+HO_2. H_2O_2 is also photodissociated when irradiated by 147 nm photons:

$$H_2O_2 + h\nu\ (147) \rightarrow OH^*(A^2\Sigma^+) + OH(A^2\Pi) \qquad (10)$$

Thus, the OH(A-X) emission (reaction 6) from H_2O_2 will also be detected. The H_2O_2 fluorescence cross section[17] at 147 nm is $(H_2O_2) = 5\times10^{-19}$ cm^2.[16] The fluorescence from photodissociation of H_2O_2 will add a background that may interfer with the data analysis. However, this additional signal in a typical experimental condition was quite small such that it is negligible as discussed below.

A summary of the experimental conditions are given in Table II. The flow velocities correspond to an average reaction time of 80 msec in the central tube. The typical concentrations of reactants are: $[CH_3OH] = 1.2\times10^{14}$, $[O_2] = 1.3\times10^{15}$ and $[Cl_2] = 5.5\times10^{13}$. Using these concentrations and assuming that wall losses for HO_2, CH_2OH and Cl are neglible so that the maximum contribution from secondary reactions can be obtained, the modeling predicts an $9.7\times10^{10} \leq [HO_2] \leq 1.9\times10^{11}$ cm^{-3} and $1.1\times10^{9} \leq [H_2O_2] \leq 4.5\times10^{9}$ cm^{-3} after 80 msec of reaction for $1\times10^{11} \leq [Cl] \leq 2\times10^{11}$ cm^{-3}. Since $[H_2O_2]$ is two-orders of magnitude smaller than $[HO_2]$, the contribution of H_2O_2 to the fluorescence is expected to be quite small if the fluorescence cross sections of HO_2 and H_2O_2 are the same order of magnitude. This is indeed true as justified below.

The fluorescence cross section of HO_2, $\sigma(HO_2)$, can be deduced from the current experimental data. CH_3OH, like HO_2 and H_2O_2, is also photodissociated by 147 nm photons to give OH*(A)

which subsequently emits in the 310 ± 10 nm region. The $\sigma(HO_2)$ can be obtained by calibration against the CH_3OH emission whose fluorescence cross section[12] at 147 nm is known, $\sigma(CH_3OH) = 3x10^{-21}$ cm^2. Using the $[HO_2]$ from the modeling, we have $5x10^{-20} \leq \sigma(HO_2) \leq 1x10^{-19}$ cm^2. Thus, $\sigma(HO_2)$ is about a factor of 5 to 10 smaller than $\sigma(H_2O_2)$. Considering the low $[H_2O_2]$, its contribution to the observed fluorescence is less than 10%. This percentage will be considerably reduced when the $[HO_2]$ is kept low.

To further verify that the [Cl] is indeed small in our experiments, and thus, the $[HO_2]$ and $[H_2O_2]$ are likewise small, the fluorescence intensity was monitored as a function of $[Cl_2]$ as shown in Fig. 3. The plot of I_f versus $[Cl_2]$ is linear for the case without or with O_3. The plots (a) and (b) are fit to the respective data, where [Cl] = 10^{11} cm^{-3} is assumed for an initial $[Cl_2] = 5.5x10^{13}$ cm^{-3} and $\sigma(H_2O_2) = 3\ \sigma(HO_2)$. This linearity extends to about three times the $[Cl_2]$ used in the HO_2+O_3 experiments (C_3H_8 was used as the OH scavenger to inhibit reaction (2) for the data when O_3 was added). If $\sigma(H_2O_2) = 10\ \sigma(HO_2)$, is assumed, the dependence deviates from the linearity as shown in plots (c) and (d). When [Cl] = $2x10^{11}$ cm^{-3} is assumed for an initial $[Cl_2] = 5.5x10^{13}$, and $\sigma(H_2O_2) = 10\ \sigma(HO_2)$ then the dependence deviates further from the linearity as shown in plots (e) and (f). For plot (f), the $H_2O_2+O_3$ reaction rate constant is assumed equal to the HO_2+O_3 reaction rate constant (Section D). If the $H_2O_2+O_3$ reaction is slower, then the nonlinearity will occur sooner at lower $[Cl_2]$. To obtain the

linear relationship, the $H_2O_2+O_3$ reaction must be faster than the HO_2+O_3 reaction, at least five times faster or at the order of 10^{-14} cm^3/s. There is no indication in the available literature that suggests this reaction rate constant to be greater than k_1. These results clearly indicate that the upper limit of the [Cl] is $2x10^{11}$ cm^{-3} and $\sigma(H_2O_2) < 10\,\sigma(HO_2)$. For a typical experimental condition, the concentrations of reactants in the central tube, where $[CH_3OH] = 1.2x10^{14}$ cm^{-3}, $[O_2] = 1.3x10^{15}$ cm cm^{-3}, and $[Cl_2] = 5.5x10^{13}$ cm^{-3}, the kinetic model predicts that the signal due to H_2O_2 is only a few percent of HO_2. Thus, the analysis of the HO_2+O_3 reaction rate constant is not significantly interferred with by the secondary product of H_2O_2.

The predicted $[HO_2]$ originating from the injector is less than $1.9x10^{11}$ cm^{-3} and the concentration of all other radical products formed in the central tube are negligible compared to $[HO_2]$, thus, the loss rate of HO_2 by other reactions is negligible when compared with the HO_2+O_3 reaction. Radical concentrations are small because, for the $[CH_3OH]$ and $[O_2]$ used in the experiment, all Cl atoms are readily converted to HO_2 within a msec and the probability for the formation of radicals involving Cl and its secondary products is thus small. The O_3 used is in the range $4x10^{14} \leq [O_3] \leq 3x10^{15}$ cm^{-3}, hence, the loss rate of HO_2 from $HO_2+HO_2 \rightarrow H_2O_2+O_2$ ($1.5x10^{-12}$ cm^3/s) is minimal when compared with HO_2+O_3. Analysis of our HO_2+O_3 reaction (Section D) at all $[O_3]$ was consistent with a psuedo-first order loss rate for HO_2.

C. Flow Tube Parameters

The flow dynamics in a flow tube reactor are complicated by

the change of pressure along the length of the tube and the change of transport velocity of radicals caused by diffusion.[18,19] The linear flow velocity in the central tube of 1 cm i.d. was about 10^3 cm/s which is 4.84 times faster than that in main reactor tube of 2.2 cm i.d.. The pressure drop will be large if the linear flow velcoity, v, is fast and the tube radius, r, is small, that is, $(\Delta p/\ell) \propto (v/r^2)$ where $(\Delta p/\ell)$ is the pressure drop across the tube length. However, even if there is a pressure drop in the central tube and hence an $[HO_2]$ gradient, the initial $[HO_2]$ at the point entering the main reaction flow tube should be constant for a given experimental set-up. This assertion is supported by the evidence that in the central tube where HO_2 is formed, a 60% change in v does not disrupt the linear dependence of $[HO_2]$ on $[Cl_2]$ (Fig. 3). The pressure gradient in the main reactor (2.2 cm i.d. and 60 cm long) is small (about 0.05). No corrections were made for this gradient, because this does not introduce any serious problem as shown in the next section.

There is no apparent complication arising from back diffusion. When the $[Cl_2]$ was increased, the $[HO_2]$ proportionally increased. If the addition of Cl_2 or increased HO_2 production caused changes in the flow velocities of the gases or the transport velocity of the radical then the linearity would not hold.

As shown in Fig. 3, changing the linear flow velocity and addition of O_3 and the OH scavenger did not affect the linear dependence of $[HO_2]$ on $[Cl_2]$. This linearity held for different

reaction distances. Such linearity again indicates a low [HO_2] and the [HO_2] is distributed uniformly in the tube. The partial pressure of the He carrier gas is at least a factor of seven greater than the sum of the partial pressures of the additive gases and at least four orders of magnitude greater than [HO_2]. Thus, the flow conditions and the gas pressures apparently constituted good mixing. This uniform distribution of [HO_2] ensures that the reaction of HO_2 with O_3 was spatially uniform in the flow tube.

The above discussion concludes that (1) there was no substantial pressure gradient in the main reactor; (2) since the [HO_2] was low (Section B), its transport velocity was the same as the carrier gas; and (3) the reactant gases were well mixed in the system. Thus, the experimental conditions were appropriate for studying the HO_2+O_3 reaction.

D. Reaction Rate Constant of HO_2+O_3

In the measurements of reaction rates, [O_3] was in the $4.5x10^{14}$ - $3x0x10^{15}$ cm^{-3} range which was much larger than the [HO_2] in the reaction flow tube. With [C_2F_3Cl] of about $3x10^{15}$ cm^{-3} or C_3H_8 of about $6x10^{15}$ cm^{-3}, reaction (2) (k_2 = $6.5x10^{-14}$ cm^3/s)[4] was negligible since it is much slower than the reaction rates of $OH+C_2F_3Cl$ ($6x10^{-12}$ cm^3/s)[4] or $OH+C_3H_8$ ($1.1x10^{-12}$ cm^3/s)[13] by about two-orders of magnitude. Thus, the decay of HO_2 due to reaction with O_3 can be represented by the psuedo-first-order approximation.

The psuedo-first order reaction rate, K, for a given [O_3] is

$$K = - v \frac{d(\ln(I_f))}{dz}$$

where v is the linear flow velocity in the main reactor, z is the reaction distance from the tip of the 1 cm tube to the HO_2 detection point in the gas cell, and I_f is proportional to $[HO_2]$. The bimolecular rate constant, k_1, is obtained from the slope of K versus $[O_3]$ since $K = k_1[O_3]$.

Sample first-order HO_2 decay plots, ($\ln(I_f)$ versus z) are shown in Figs. 4 and 5 with C_2F_3Cl and C_3H_8 as the OH scavengers, respectively. For each experimental run, the movable HO_2 injector was moved 50 cm at 5-cm intervals. The z=0 points in Figs. 4 and 5 were set at about 6 cm from the HO_2 detection point. The reaction time between HO_2+O_3 was increased for each increase in distance. Each plot was linear for the range of $0 \leq [O_3] \leq 3\times10^{15}$ cm^{-3} used in these experiments which indicate that (i) the OH product from reaction (2) was effectively removed by the scavengers, and (ii) HO_2+HO_2 reaction is negligible as indicated by the small decrease rate of $[HO_2]$ at $[O_3]=0$. This is consistent with predicted $[HO_2] \leq 1\times10^{11}$ molecule/cm^3. The experimental data is summarized in Table II.

The first-order rates of reaction (1) versus $[O_3]$ are shown in Figs. 6 and 7 for C_2F_3Cl and C_3H_8 as OH scavengers, respectively. The vertical error bars represent one standard deviation which includes the uncertainties in the determination of v and the linear least square fit of $\ln(I_f)$ versus z (as in Figs. 4 and 5). The horizontal error bars represent the standard deviation in determining $[O_3]$. The lines are linear least squares fit. The bimolecular rate constants obtained from the slopes of Figs. 6 and 7 are 1.7×10^{-15} and 2.0×10^{-15} cm^3/s, respectively. A reasonable estimate of the precision is about

17% using a 95% confidence level from the errors: k_1 (±10%), K (±10%), [O_3] (±5%), and v (±9%). Adding a systematic error of 10%, the experimental resultant error is 20%. The intercepts represent HO_2 loss to the walls of the reactor. The intercept of K_o = 0.3 s^{-1} in Fig. 6 and ∿ 0 in Fig. 7 are quite small, suggesting the apparent HO_2 loss due to the walls being quite small.

The reaction rate constants were also measured using a flow tube of 4.8 cm i.d. The results are shown in Fig. 8. With C_2F_3Cl as the OH scavenger, the slope gave k_1 = (1.5 ± 0.4)x10^{-15} cm^3/s, and with C_3H_8, k_1 = (2.1 ± 0.5)x10^{-15} cm^3/s. The experimental uncertainties for the measurements with such large flow tube are relatively high. The flow velocity and the gas mixing in a large flow tube are more difficult to control than that of a small tube. Nevertheless, k_1 values obtained from the larger flow tube are in agreement with the small one.

IV. CONCLUSION

The current k_1 value at room temperature (298 K) determined from Figs. 6 and 7 is (1.9±0.3)x10^{-15} cm^3/s, where error limit represents 95% confidence limit. This is in good agreement with the absolute rate constant of 2x10^{-15} cm^3/s measured by the LMR method[4] and the value of 1.7x10^{-15} cm^3/s indirectly measured by photolysis of dry H_2-O_2-O_3 mixtures.[9] In the indirect measurements , k_1 was determined from relative rates with the $2HO_2 \rightarrow H_2O_2+O_2$ reaction as the competing reaction. The lower k_1 values derived from relative rates from early photolysis

results[7,8] were reconciled to the later detemination[9] by taking into account that in the presence of water vapor the self-reaction of HO_2 increases.

The Arrhenius parameters in the temperature range 230-365 K indicate a low value for the A-factor (1.3×10^{-14} cm^{-3}/s) for a simple atom-transfer mechanism.[4] The reaction rate constants at different temperatures will be further measured in our laboratory to verify the Arrhenius parameters. The reaction rate constants at various temperature are needed in the stratospheric modeling, since temperature changes with height in the stratosphere.

ACKNOWLEDGEMENT

The authors wish to thank Dr. W. B. DeMore, D. L. F. Keyser, Dr. M. T. Leu, and Dr. M. J. Molina at the Jet Propulsion Laboratory, Dr. C. J. Howard at the NOAA Environmental Research Laboratory, Dr. D. M. Golden at the SRI International, Dr. R. F. Hampson at the National Bureau of Standard, and Dr. J. B. Nee, Dr. W. C. Wang and Dr. X. Y. Wang in our laboratory for useful discussion and suggestions. The HO_2 detection method is based on the work supported by the NSF under Grant No. ATM-8412618. This work is supported by the NASA under Grant No. NAGW-661.

Table I

Number	Reactions	Rate Constants (cm^3/molec. -s)
1	$CH_3OH + Cl \rightarrow CH_2OH + HCl$	6.30 E-11[a]
2	$CH_2OH + O_2 \rightarrow CH_2O + HO_2$	1.40 E-12
3	$CH_2OH + Cl \rightarrow CH_2O + HCl$	3.00 E-10[b]
4	$HO_2 + HO_2 \rightarrow H_2O_2 + O_2$	1.50 E-12
5	$Cl + H_2O_2 \rightarrow HCl + HO_2$	4.10 E-13
6	$Cl + HO_2 \rightarrow HCl + O_2$	3.20 E-11
7	$Cl + HO_2 \rightarrow ClO + OH$	9.10 E-12
8	$OH + HO_2 \rightarrow H_2O + O_2$	7.00 E-11
9	$OH + H_2O_2 \rightarrow H_2O + HO_2$	1.70 E-12
10	$ClO + HO_2 \rightarrow HOCl + O_2$	5.00 E-12
11	$OH + HCl \rightarrow H_2O + Cl$	6.60 E-13
12	$ClO + OH \rightarrow Cl + HO_2$	1.20 E-11
13	$ClO + ClO \rightarrow Cl + CLO_2$	1.60 E-14
14	$ClO + ClO \rightarrow Cl_2 + O_2$	7.80 E-15
15	$OH + HOCl \rightarrow H_2O + ClO$	1.80 E-12
16	$OH + CH_3OH \rightarrow H_2O + CH_2OH$	1.00 E-12
17	$Cl + CH_2O \rightarrow HCl + HCO$	7.30 E-11
18	$HCO + O_2 \rightarrow CO + HO_2$	5.50 E-12
19	$Cl + HOCl \rightarrow Cl_2 + OH$	1.90 E-12
20	$Cl + O_2 \rightarrow ClO_2$	4.90 E-17[c]
21	$Cl + ClO_2 \rightarrow Cl_2 + O_2$	1.40 E-10
22	$Cl + ClO_2 \rightarrow ClO + ClO$	8.00 E-12
23	$OH + CH_2O \rightarrow H_2O + HCO$	1.00 E-11
24	$HO_2 + CH_2O \rightarrow$ Adduct	4.50 E-14[d]
25	$HO_2 +$ wall $\rightarrow$ products	$k_w(HO_2)$[e]
26	$CH_2OH +$ wall $\rightarrow$ products	$k_w(CH_2OH)$
27	Cl + Wall $\rightarrow$ products	$k_w(Cl)$

(continued) Table I

[a] All reactions unless otherwise stated are similar to those considered in Reference 15 and the rate constants compared with Reference 16. The rate constant 6.30 E-11 reads 6.30×10^{-11}.

[b] Added to the list of reactions, while a negligible step in comparison to the CH_2OH+O_2 reaction because of our high $[O_2]$, this step was necessary in the simulation of the data in Reference 6. The gas kinetic value was assumed for the rate constant.

[c] $Cl + O_2 + M \rightarrow ClO_2 + M$ with M principally He at 1.5 torr.

[d] Added to list for completion.

[e] Wall lost rates. See text.

Table II

Summary of Experimental Conditions*

Run	$[O_3]$ (10^{15} cm^{-3})	$[Cl_2]$ (10^{13} cm^{-3})	$[CH_3OH]$ (10^{14} cm^{-3})	$[O_2]$ (10^{15} cm^{-3})	$[C_2F_3Cl]$ (10^{15} cm^{-3})	P** (torr)	v (cm/s)	$d(\ln I_f)/dz$ (10^{-2} cm^{-1})
1	0	5.70	1.11	1.43	3.34	1.633	203	0
2	0.451	5.64	1.13	1.43	3.69	1.699	216	0.35
3	0.830	5.57	1.13	1.43	3.60	1.687	173	1.02
4	1.16	5.57	1.23	1.46	3.53	1.651	165	1.52
5	1.34	5.51	1.12	1.39	3.50	1.690	183	1.18
6	1.73	5.24	1.10	1.43	3.56	1.664	190	1.85
7	2.13	5.51	1.13	1.30	3.50	1.834	190	2.20
8	2.43	3.11	1.10	1.36	3.43	1.717	197	2.34
9	3.00	4.54	1.44	1.04	3.18	1.714	235	2.54
					$[C_3H_8]$ (10^{15} cm^{-3})			
10	0	5.90	1.21	1.30	6.40	1.700	220	0
11	0.642	5.51	1.20	1.33	4.86	1.820	197	0.66
12	1.25	5.44	1.31	1.26	5.35	1.882	198	1.11
13	1.52	6.80	1.27	1.39	5.51	1.916	189	1.54
14	1.99	6.03	1.22	1.52	6.61	1.890	171	2.20
15	2.25	6.03	1.18	1.30	6.22	1.960	172	2.50
16	2.61	6.22	1.26	1.33	6.42	2.051	175	3.02

*tube radius is 2.2 cm i.d.

**total cell pressure

REFERENCES

1. J. G. Anderson and F. Kaufman, Chem. Phys. Lett. 19, 483 (1973).

2. M. J. Kurylo, Chem. Phys. Lett. 23, 467 (1973).

3. A. R. Ravishankara, P. H. Wine, and A. D. Langford, J. Chem. Phys. 70, 984 (1979).

4. M. S. Zahniser and C. J. Howard, J. Chem. Phys. 73, 1620 (1980).

5. M. Suto and L. C. Lee, J. Chem. Phys. 80, 195 (1984).

6. W. C. Wang, M. Suto and L. C. Lee, J. Chem. Phys. 81, 3122 (1984), and references there-in.

7. W. B. DeMore and E. Tschuikow-Roux, J. Phys. Chem. 78, 1447 (1974).

8. R. Simonaitis and J. Heicklen, J. Phys. Chem., 77, 1932 (1973).

9. W. B. DeMore, J. Phys. Chem. 83, 1113 (1979).

10. R. J. Cvetanovic, D. L. Singleton, and G. Paraskevopoulous, J. Phys. Chem. 83, 50 (1979).

11. L. C. Lee and Masako Suto, K. Y. Tang, J. Chem. Phys. 84, 0000 (1986).

12. J. B. Nee, M. Suto, and L. C. Lee, Chem. Phys. 98, 147 (1985).

13. M. Suto and L. C. Lee, unpublished.

14. A. C. Hindmarch, "LSODE", Lawrence Livermore Laboratory, University of California, Livermore, CA; A. C. Hindmarch, ACM-Signum Newslett. 15, 10 (1980).

15. G. A. Takacs and C. J. Howard, J. Phys. Chem. 88, 2110 (1984).

16. W. B. DeMore, J. J. Margitan, M. J. Molina, R. T. Watson, D. M. Golden, R. F. Hampson, M. J. Kurylo, C. J. Howard, and A. R. Ravishankara, Evaluation Panel, Chemical Kinetics and Photochemical Data for Use in Stratospheric Modeling, JPL, Publication 85-37 (1985).

17. M. Suto and L. C. Lee, Chem. Phys. Lett. 98, 152 (1983).

18. F. Kaufmann, Prog. React. Kinet. 1, 3 (1961).

19. C. J. Howard, J. Phys. Chem. 83, 3 (1979).

FIGURE CAPTIONS

Figure 1 Schematic diagram of experimental apparatus.

Figure 2 Emission intensity versus $[CH_3OH]$ with $[Cl_2]$ = 5.5×10^{13} cm^{-3} and $[O_2]$ = 1.3×10^{15} cm^{-3}, for a reaction time of 65 msec (■) and 45 msec (●) in the central tube. See text for discussion.

Figure 3 I_f versus $[Cl_2]$. Concentrations in cm^{-3}: $[O_3]$ = 0, $[CH_3OH]$ = 1.1×10^{14}. $[O_2]$ = 1.3×10^{15}, v = 292 cm/s (●); $[O_3]$ = 2.0×10^{15}, $[CH_3OH]$ = 1.2×10^{14}, $[O_2]$ = 1.3×10^{15}, $[C_3H_8]$ = 6.4×10^{15}, v = 183 cm/s (■), for z = 20 cm. (a) - (f) are the modeling curves (see text).

Figure 4 First order decay plots with C_2F_3Cl as OH scavenger. See Table II for experimental condition: (a) run 1, $[O_3]$ = 0; (b) run 3, $[O_3]$ = 8.30×10^{14} cm^{-3}; (c) run 7, $[O_3]$ = 2.13×10^{15} cm^{-3}.

Figure 5 First order decay plots with C_3H_8 as the OH scavenger. See Table II for experimental condition (a) run 11, $[O_3]$ = 6.42×10^{14} cm^{-3}, (b) run 12, $[O_3]$ = 1.25×10^{15} cm^{-3}, and (c) run 15, $[O_3]$ = 2.25×10^{15} cm^{-3}.

Figure 6 K versus $[O_3]$ with C_2F_3Cl as the OH scavanger. The tube radius was 2.2 cm i.d. The slope is k_1 = 1.7×10^{-15} cm^3/s.

Figure 7 Same as Figure 6 but with C_3H_8 as the OH scavanger, k_1 = 2.0×10^{-15} cm^3/s.

Figure 8 K versus $[O_3]$. The tube radius was 4.8 cm i.d. The slope is k_1. Plot (a) with C_2F_3Cl as the OH scavenger, k_1 = $(1.5 \pm 0.4) \times 10^{-15}$ cm^3/s and plot (b) with C_3H_8, k_1 = $(2.1 \pm 0.5) \times 10^{-15}$ cm^3/s.

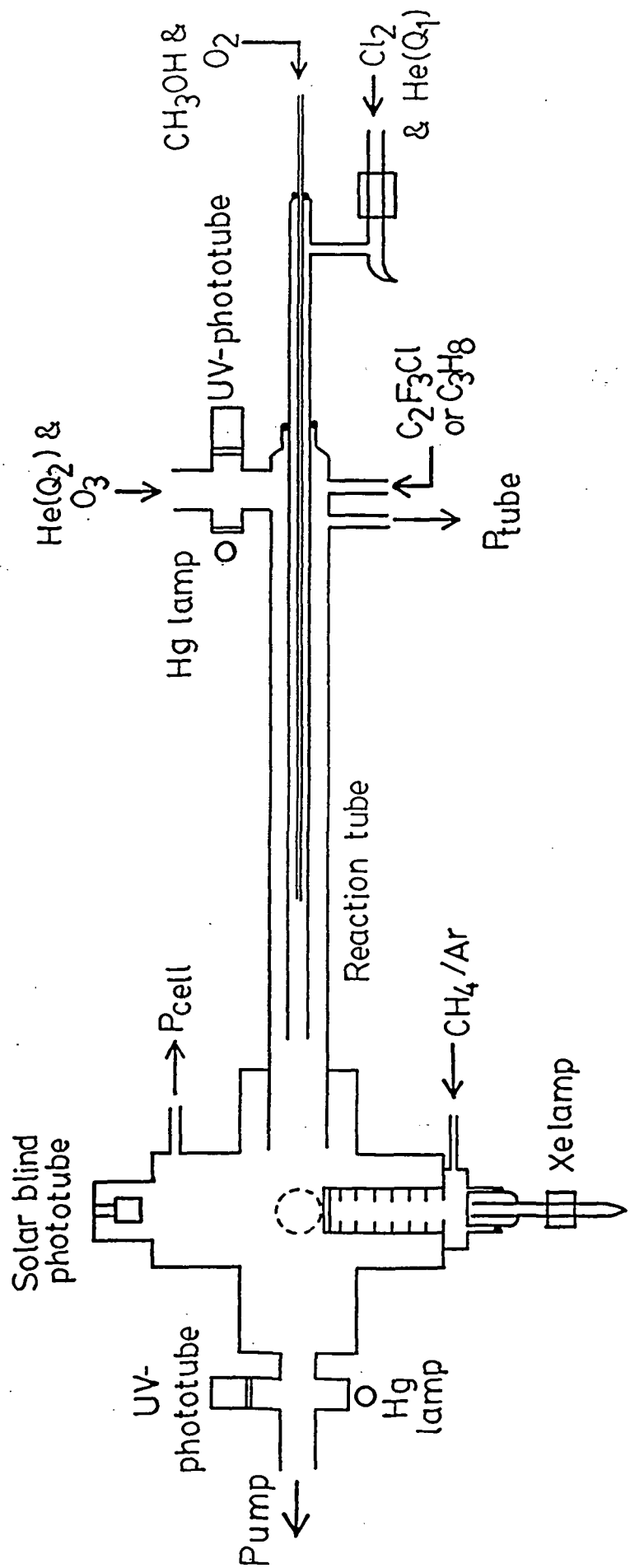
CH_3OH & O_2
Cl_2 & $He(Q_1)$
UV-phototube
$He(Q_2)$ & O_3
Hg lamp
C_2F_3Cl or C_3H_8
P_{tube}
Reaction tube
P_{cell}
CH_4 /Ar
Xe lamp
Solar blind phototube
UV-phototube
Hg lamp
Pump

Fig. 1

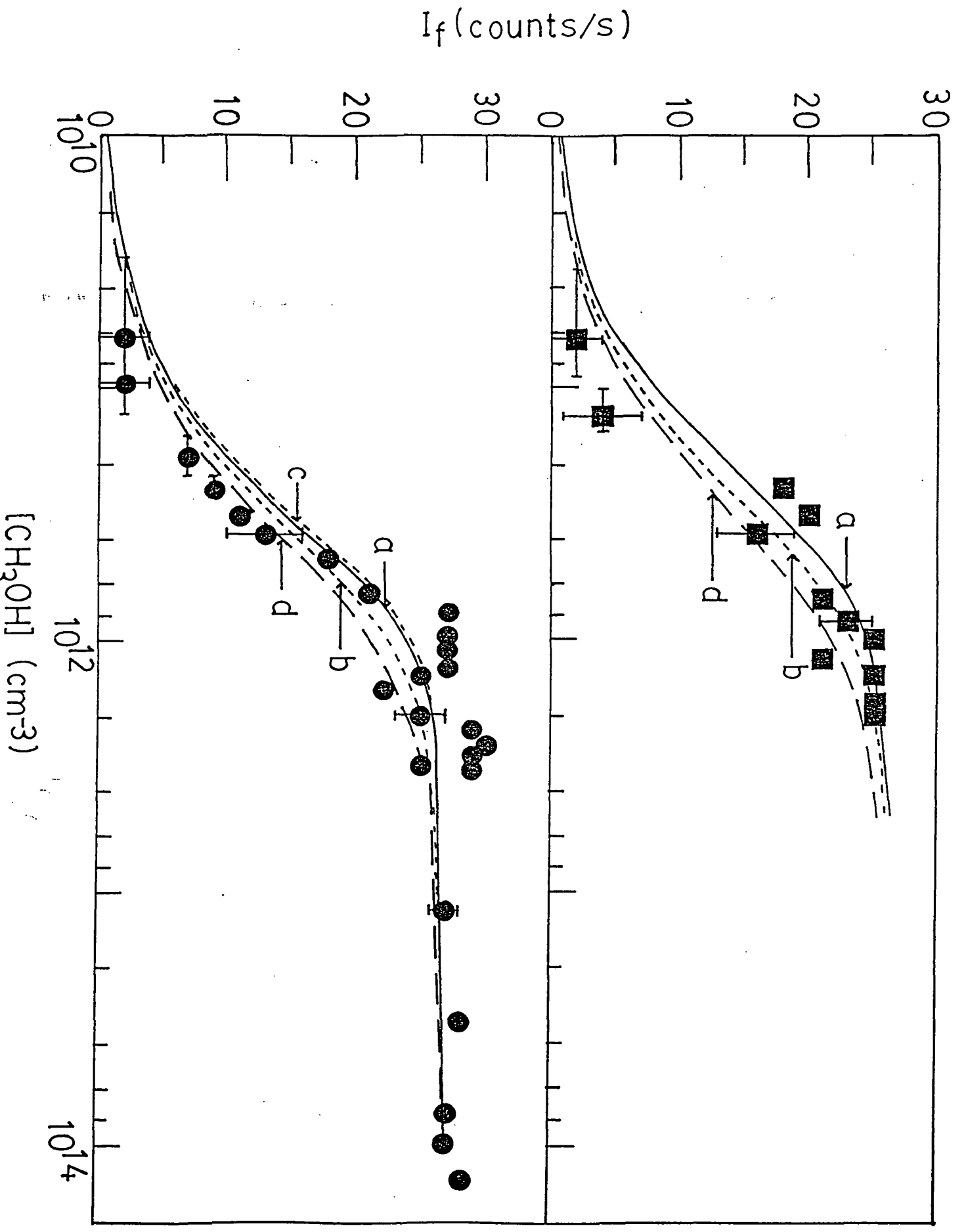

Fig. 2

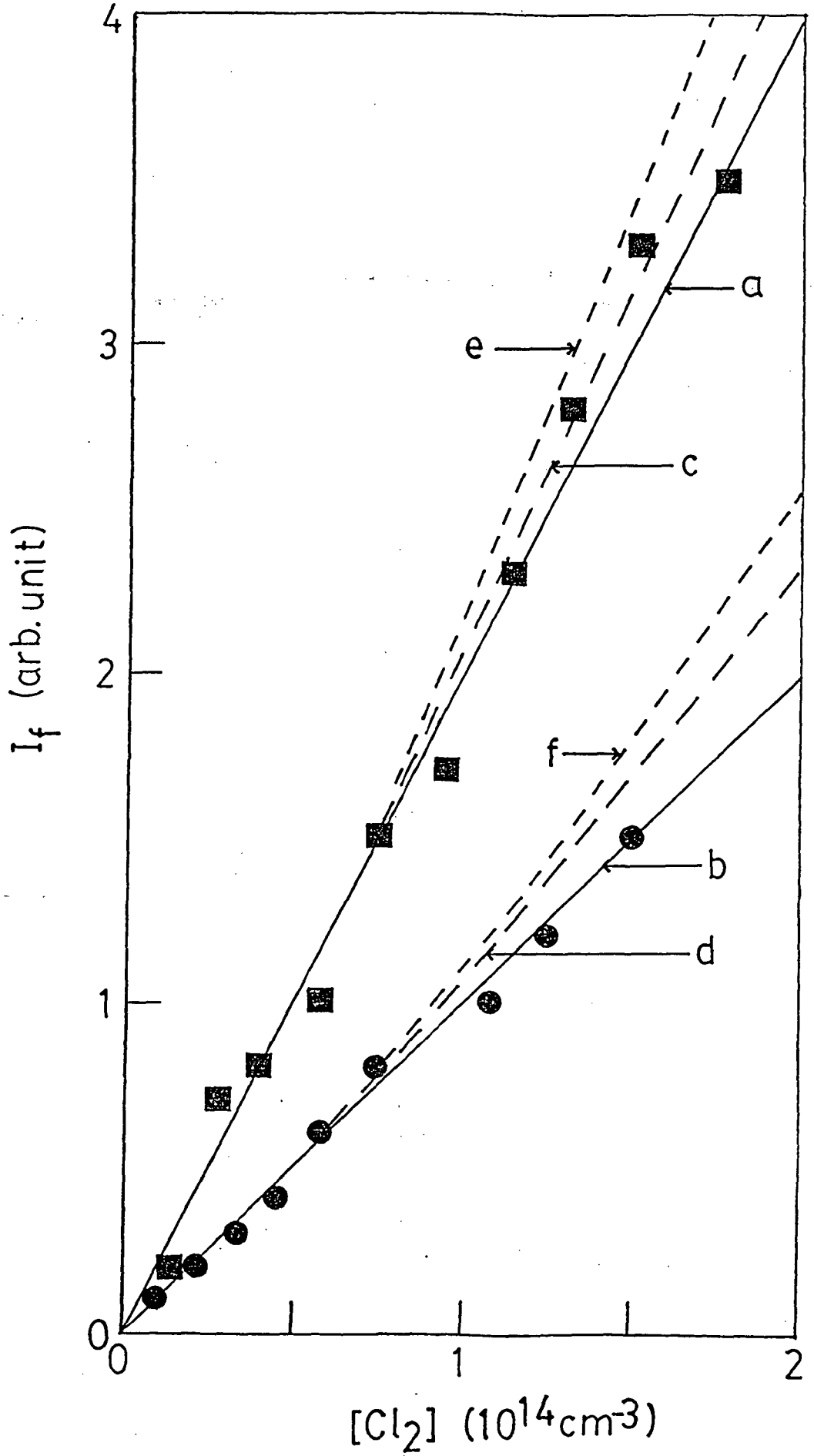
4
3
2
1
0
0
1
2
I_f (arb. unit)
$[Cl_2]$ $(10^{14} cm^{-3})$
a
b
c
d
e
f

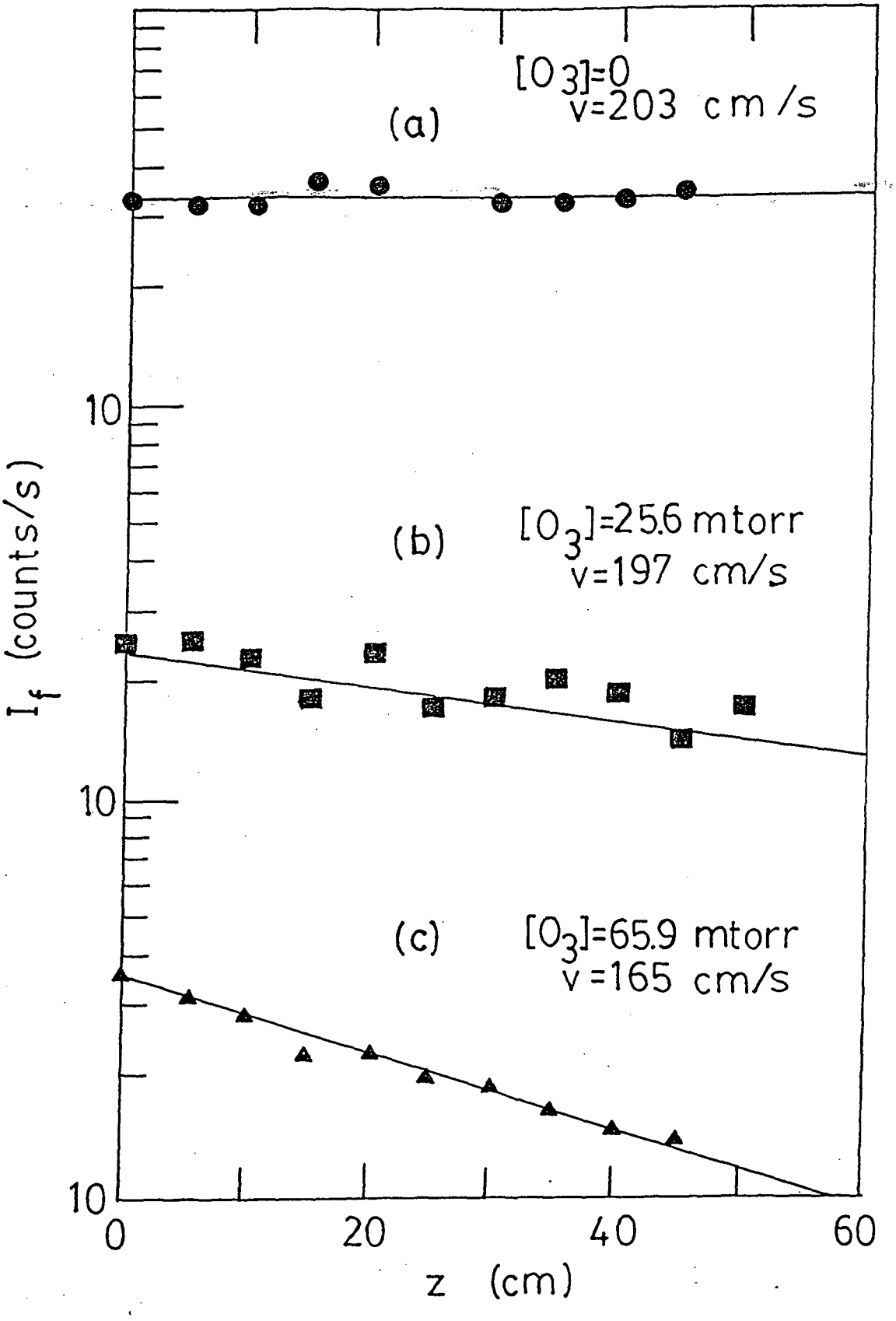
[O3]=0
v=203 cm/s
(a)
[O3]=25.6 mtorr
v=197 cm/s
(b)
[O3]=65.9 mtorr
v=165 cm/s
(c)
If (counts/s)
10
10
10
0
20
40
60
z (cm)

Fig. 4

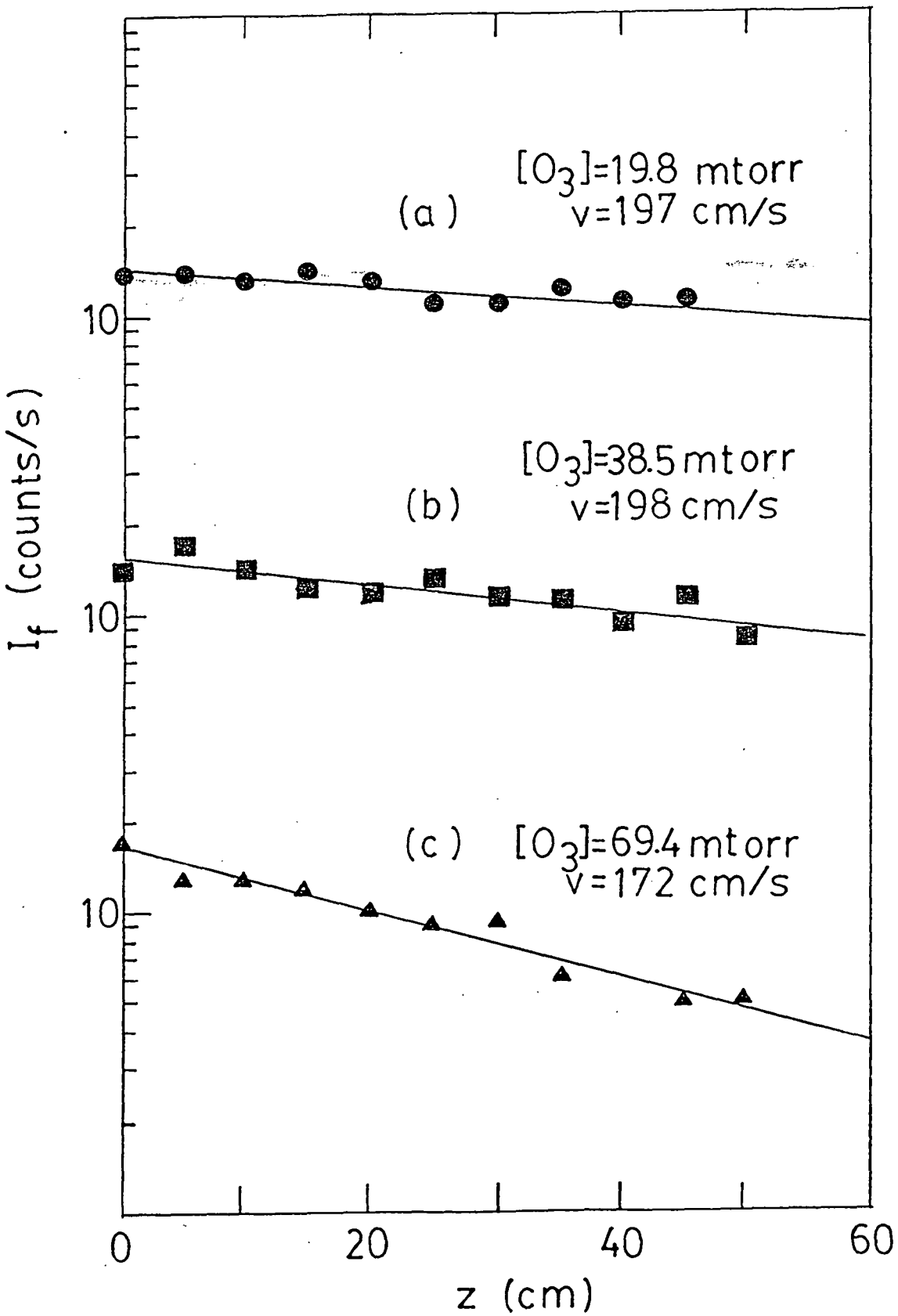
[O3]=19.8 mtorr
v=197 cm/s
(a)
[O3]=38.5 mtorr
v=198 cm/s
(b)
(c) [O3]=69.4 mtorr
v=172 cm/s
10
10
10
If (counts/s)
0
20
40
60
z (cm)

Fig. 5

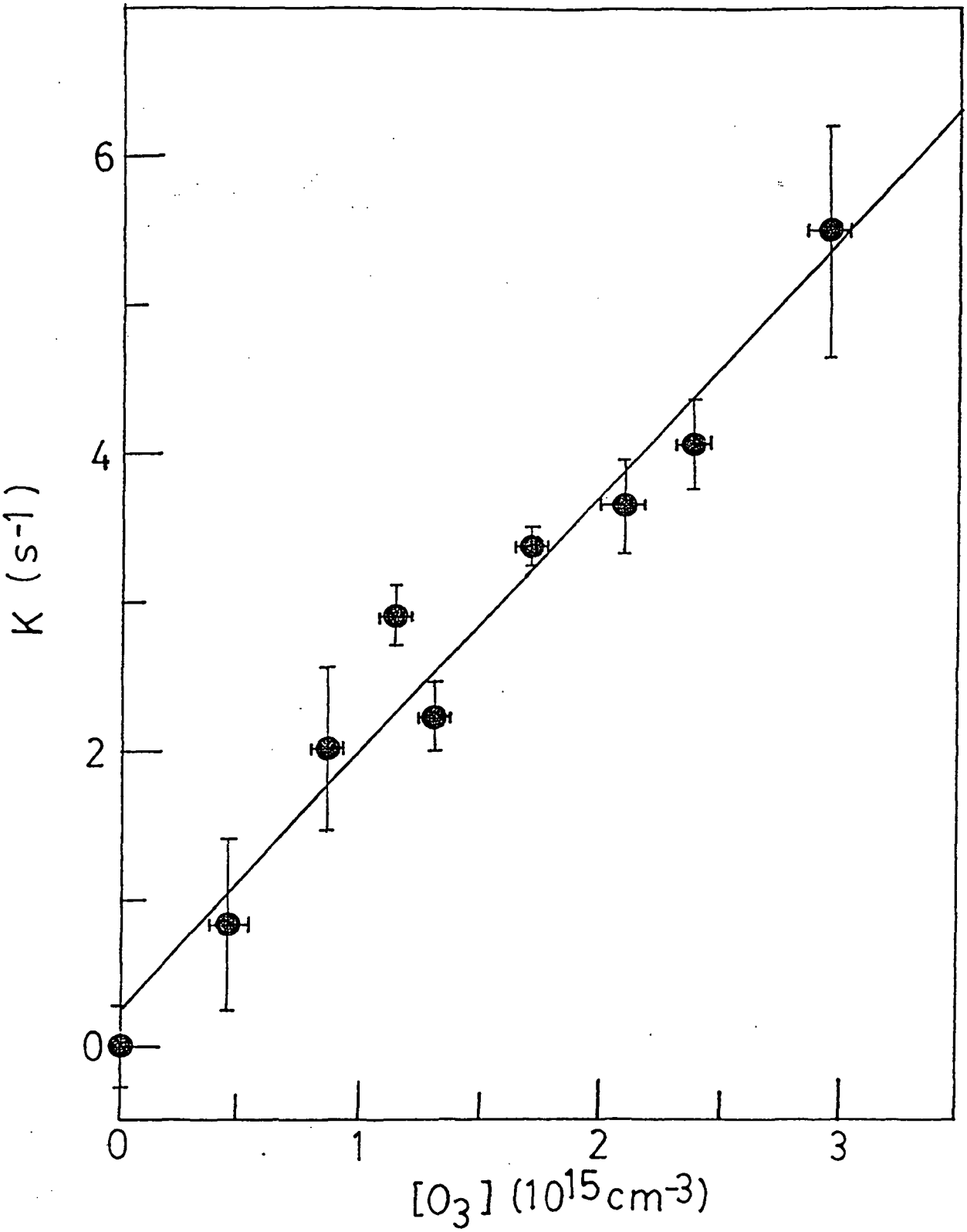

Fig. 6

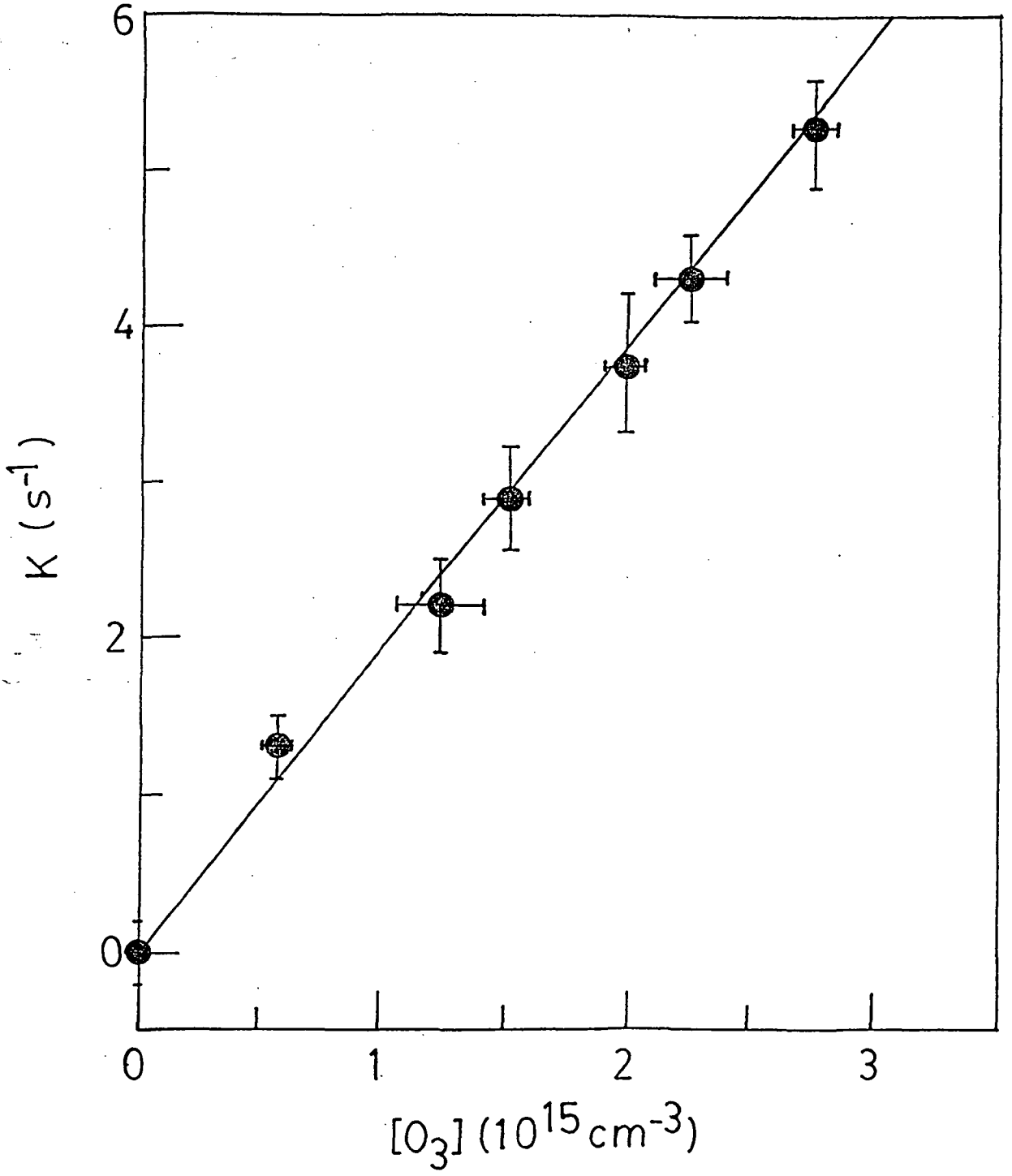

Fig. 7

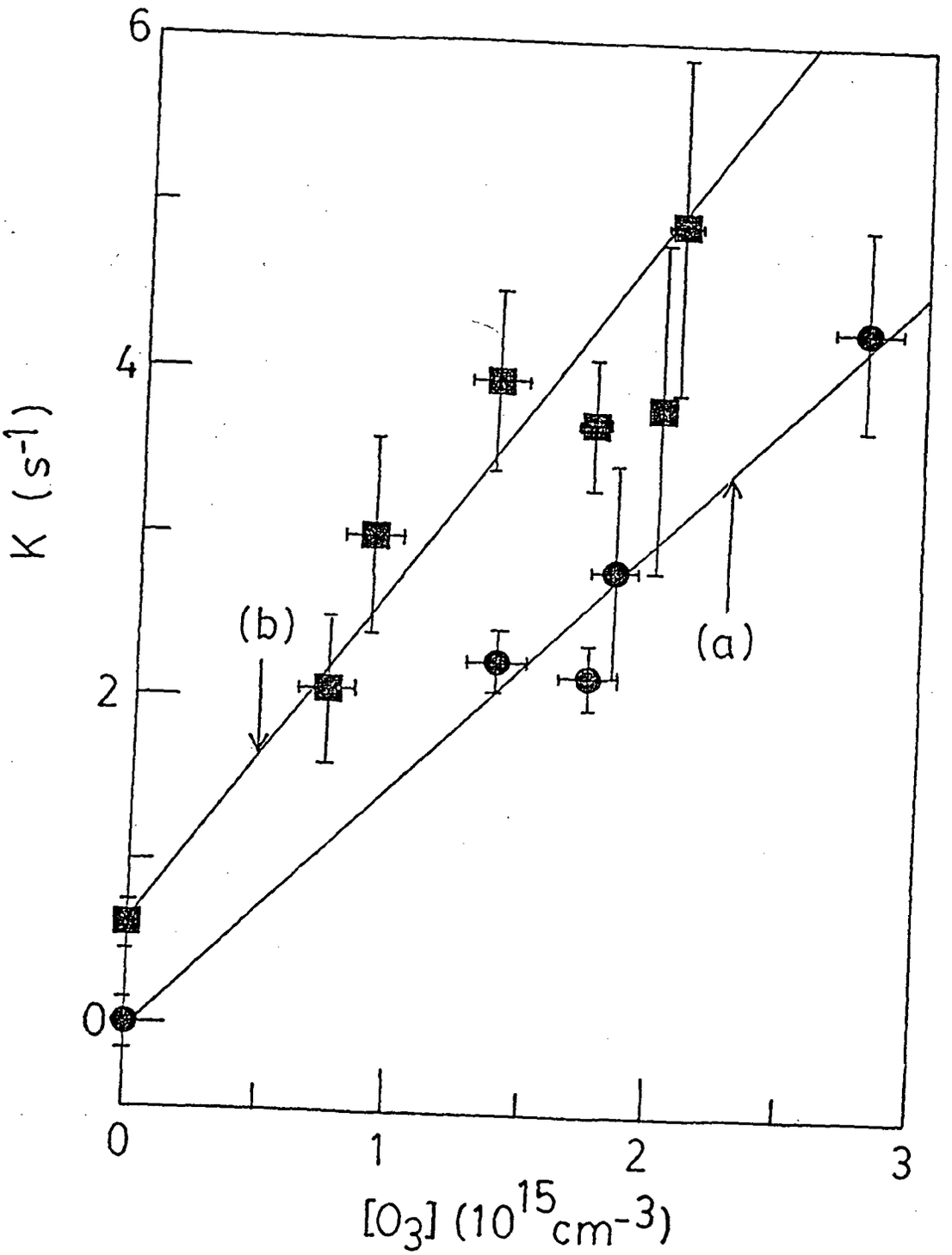

Fig. 8